ADVANCED QUANTUM TECHNOLOGIES
www.advquantumtech.com

Extending Quantum Links: Modules for Fiber- and Memory-Based Quantum Repeaters

Peter van Loock, Wolfgang Alt, Christoph Becher, Oliver Benson, Holger Boche, Christian Deppe, Jürgen Eschner, Sven Höfling, Dieter Meschede,* Peter Michler, Frank Schmidt, and Harald Weinfurter*

Elementary building blocks for quantum repeaters based on fiber channels and memory stations are analyzed. Implementations are considered for three different physical platforms, for which suitable components are available: quantum dots, trapped atoms and ions, and color centers in diamond. The performances of basic quantum repeater links for these platforms are evaluated and compared, both for present-day, state-of-the-art experimental parameters as well as for parameters that can in principle be reached in the future. The ultimate goal is to experimentally explore regimes at intermediate distances—up to a few 100 km—in which the repeater-assisted secret key transmission rates exceed the maximal rate achievable via direct transmission. Two different protocols are considered, one of which is better adapted to the higher source clock rate and lower memory coherence time of the quantum dot platform, while the other circumvents the need of writing photonic quantum states into the memories in a heralded, nondestructive fashion. The elementary building blocks and protocols can be connected in a modular form to construct a quantum repeater system that is potentially scalable to large distances.

1. Introduction

Quantum key distribution (QKD) and related schemes are offering a paradigm change in establishing secure communication: algorithmic security is replaced by physically secure generation of encryption keys.[1] The symmetric keys created by QKD can be used to securely transmit messages between two stations (Alice and Bob) via public channels. Security is warranted by physically detecting any eavesdropping attack. To generate a key, the iconic BB84 protocol[2] employs nonorthogonal quantum states of photons carrying qubit information, while other schemes make use of measuring entangled photon pairs, such as the Ekert protocol.[3] More generally, establishing entanglement of distant quantum objects provides a critical resource for efficient distribution of quantum information, both at short and long distances;

Prof. P. van Loock, F. Schmidt
Institute of Physics
Johannes Gutenberg University Mainz
Staudingerweg 7, Mainz 55128, Germany
E-mail: loock@uni-mainz.de

Dr. W. Alt, Prof. D. Meschede
Institute of Applied Physics
University of Bonn
Wegelerstraße 8, Bonn 53115, Germany
E-mail: meschede@uni-bonn.de

Prof. C. Becher, Prof. J. Eschner
Fachrichtung Physik
Universität des Saarlandes
Campus E2.6, Saarbrücken 66123, Germany

Prof. O. Benson
Institut für Physik
Humboldt-Universität zu Berlin
Newtonstr. 15, Berlin 12489, Germany

Prof. O. Benson
IRIS Adlershof
Humboldt-Universität zu Berlin
Zum Großen Windkanal 6, Berlin 12489, Germany

Prof. H. Boche
Lehrstuhl für Theoretische Informationstechnik
Technische Universität München
München 80290, Germany

Prof. H. Boche
Munich Center for Quantum Science and Technology (MCQST)
München 80799, Germany

Dr. C. Deppe
Lehrstuhl für Nachrichtentechnik
Technische Universität München
München 80290, Germany
(Affil Cont)

The ORCID identification number(s) for the author(s) of this article can be found under https://doi.org/10.1002/qute.201900141

DOI: 10.1002/qute.201900141

(affiliation continued on next page)

applications beyond quantum cryptography, such as distributed quantum information processing and future quantum networks,[4] will also depend on this resource.

Networks based on individual point-to-point links (PPLs) over 50–80 km length have been realized at the metropolitan area level, and even a long distance connecting Beijing and Shanghai (≈2.000 km) has been bridged via 32 intermediate stations.[5] So far, however, such networks rely on independent quantum PPLs chained together by "trusted nodes," connecting the links by classical operations ("receive and resend") and thus providing full access to the transmitted bits at each node. Truly long-range quantum links have been realized via satellite channels,[6] yet up to now also the satellites serve as trusted nodes in such schemes. Moreover, since these links require large-scale send-and-receive facilities, it is likely that they need to be combined with "local-area" ground-based quantum networks (of a smaller, intermediate range) as obtainable from the elementary fiber-based schemes presented and discussed here.

At present the main obstacle in establishing large-scale quantum networks are inherent losses of the transmission channels. The current record for terrestrial, fiber-based point-to-point QKD lies in the range of about 400 km.[7,8] As a consequence,[9] secret key rates (SKRs) obtained via direct transmission (without intermediate stations) through an optical quantum channel of length L are effectively limited by the channel transmission efficiency $\eta = \exp(-L/L_{\text{att}})$ for large L where L_{att} is the attenuation length of the channel.[10] More precisely, this limit corresponds to a secret key capacity of 1.44 η (per channel use and per mode, in units of secret bits[11]).[12] In particular, optical fiber systems feature a loss rate of about 0.2 dB km^{-1} (corresponding to $L_{\text{att}} = 22$ km), limiting useful distances to a few hundred km (**Figure 1**).

There are interesting methods to overcome this limitation without the use of quantum memories by sending fairly simple quantum states (in the form of single photons or optical coherent states) to a detector station placed in the middle of the channel.[14,15] Especially the "twin-field QKD" concept[15] is appealing, as it needs[16] neither multiple parallel channel transmissions nor nondestructive measurements with feedforward and multiplexing,[14] but instead only transmission of phase-sensitive single-mode quantum states and their interference at the middle station. Experimental proof-of-principle demonstrations of the twin-field concept were reported very recently.[17–19] Both approaches[14,15] reduce the effective channel length by a factor of two, corresponding to an enhanced transmission efficiency of $\sqrt{\eta} = \exp[-(L/2)/L_{\text{att}}]$. However, neither of them has been shown to be scalable to larger distances by further improving the effective transmission. In principle, there are other, all-optical approaches for long-distance, even scalable quantum communication with no need for storing qubits in matter-based memories, but such schemes depend on the engineering of complex multiphoton (entangled) quantum states and a sufficiently close spacing of stations along the channel (every 1–5 km) in order to exploit the sophisticated concept of quantum error correction codes.[20]

Therefore, it is currently assumed that the most feasible and promising route toward long-distance quantum communication, while entirely avoiding trusted node configurations, is based upon the use of quantum repeaters (QRs)[21] that include intermediate stations (typically every 10–100 km) equipped with quantum memories realized by atomic or solid-state qubits. Here, we consider elementary fiber- and memory-based schemes, which we refer to as quantum repeater cells (QR cells). By storing quantum states for sufficiently long, these schemes allow to enter the rate regime[13] between η and $\sqrt{\eta}$ and may serve as modular building blocks for bridging larger distances. Thus, ultimately, true quantum networks based on quantum repeaters should not only eliminate the need to trust the stations along the channels of the network but also achieve a QKD rate scaling with distance at least as efficient as a trusted relay or

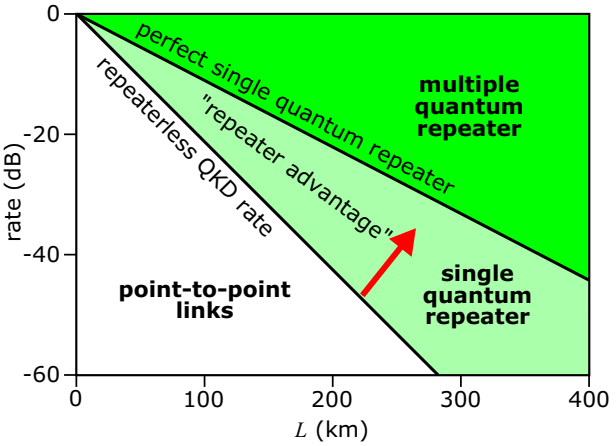

Figure 1. QKD rate in dB (normalized to the protocol's clock rate) as a function of distance in km. Point-to-point protocols scale as $\sim \eta = \exp(-\frac{L}{L_{\text{att}}})$, limited by the "repeaterless" bound.[12] For telecom fibers: $L_{\text{att}} = 22$ km. An ideal "single" quantum repeater with only one middle station[13] scales as $\sim \sqrt{\eta} = \exp(-\frac{L/2}{L_{\text{att}}})$. "Multiple" repeaters may further reduce the effective loss and extend the transmission distance. The exact "repeaterless" bound (secret key capacity) is $-\log_2(1-\eta) \approx 1.44\eta$ in units of secret bits,[12] where the approximation only holds for sufficiently small η (large distances).

Prof. S. Höfling
Technische Physik
Physikalisches Institut und Wilhelm Conrad Röntgen Center for Complex Material Systems
Universität Würzburg
Am Hubland, Würzburg 97074, Germany

Prof. P. Michler
Institut für Halbleiteroptik und Funktionelle Grenzflächen (IHFG)
Center for Integrated Quantum Science and Technology (IQST) and SCoPE
University of Stuttgart
Allmandring 3, Stuttgart 70569, Germany

Prof. H. Weinfurter
Fakultät für Physik
Ludwig-Maximilians-Universität München
Schellingstr. 4, München 80799, Germany

Prof. H. Weinfurter
Munich Center for Quantum Science and Technology (MCQST)
München 80799, Germany

Prof. H. Weinfurter
Max-Planck Institut für Quantenoptik
Hans-Kopfermann-Str. 1, Garching 85748, Germany

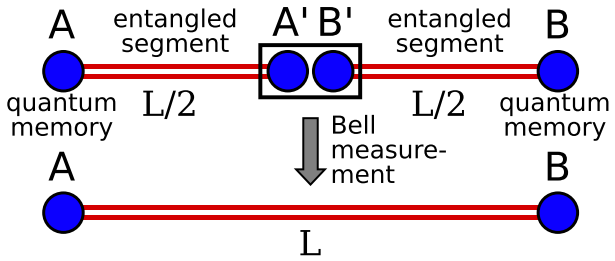

Figure 2. Generic QR link for increasing the communication distance. Initially, for each segment AA′ and B′B, quantum memories (full circles) are entangled with each other (double red line) over a distance $L/2$. Via a Bell-state measurement (black box) on the two memories in the central repeater node, the entanglement is swapped to the outer memories A and B separated by distance L. Thus, a new, longer segment is created that is usable for further extensions of the quantum link by repeated concatenation of this procedure including some form of quantum error detection or correction.

an entanglement distribution rate scaling more efficient than a quantum relay where each node only measures optical quantum states without storing them. Compared with quantum PPLs chained together by trusted nodes and other forms of quantum relays, genuine repeater-based quantum networks would thus represent a leap both conceptually and quantitatively.

The first QR concepts were proposed already 20 years ago[21] to overcome the distance limitation by distributing, enhancing, and connecting short-range entanglement through local quantum operations and classical communication. In the simplest case, quantum correlations from two entangled point-to-point segments AA′ and B′B are connected via a collective Bell-state measurement (BM) at the central "repeater" node A′B′, resulting in so-called entanglement swapping to nodes A and B (**Figure 2**). These larger segments can then be concatenated further in the same way, while a simple multiplication of the channel transmission efficiencies per segment and a propagation and accumulation of errors can be prevented by storing quantum information in quantum memories and applying entanglement purification on many entangled pairs in each segment[21] or incorporating quantum error correction codes into the memory qubits.[20] Overcoming the distance and rate limitations in a scalable fashion, QRs offer highly attractive functionality for future long-range quantum networks.[22]

Experimentally, QRs have remained an enormous challenge up to now.[20,23] A QR constitutes a system based on several different hardware components. Although all necessary components have been demonstrated to some extent individually, combining these into a fully operational (and hence scalable) repeater system is demanding and first experimental demonstrations in this direction are now only beginning to be reported.[24]

One of the most critical hardware components are the quantum memories required to effectively synchronize the arrival of quantum information for further processing at the individual nodes. Depending on the range and the application of the repeater system, the required memory coherence times vary. For example, in order to establish entanglement over 1000 km via a standard QR[21] at least millisecond storage times are needed only to be able to cover the waiting time for a classical signal sent over the total distance. In a fully nested quantum repeater with probabilistic entanglement purification and swapping steps including two-way classical communication, even longer storage times will be required.[25] Deterministic entanglement swapping and quantum error correction of local gate and memory errors may reduce these requirements,[20] but most memory systems are still not sufficiently long-lived or fault-tolerant.[26]

Here we analyze small-scale, functional QR systems that may serve as elementary building blocks for experimental QR realizations on a larger scale. Implementations are considered for three different physical platforms, for which suitable components are available: quantum dots, trapped atoms and ions, and color centers in diamond. The aim of these elementary schemes is to experimentally approach a regime at intermediate distances (up to several 100 km) in which the qubit transmission and secret key rates exceed the limits of direct transmission. Based on a simple model we compare the properties of the different platforms capturing the influence of source and memory efficiencies on the repeater performance for each system.

In order to assess and compare the specific capabilities of each platform, we primarily consider the most dominating and distinct effects in a typical elementary QR, namely, transmission loss in the fiber channel and memory dephasing at the repeater stations. In addition, we do include source and detector efficiencies, but we omit, for example, detector dark counts. These have a significant impact on secret key rates for larger distances.[27] The overall performance of the source includes an experimentally determined efficiency and a clock (repetition) rate whose influence on the repeater rates depends on the repeater protocol.

The memory quality is given by an experimentally determined coherence time, but the impact of memory dephasing errors on the entanglement fidelity and thus the secret key fraction can be controlled by a freely chosen, so-called memory cutoff time.[28] This means a quantum state is never kept in the memory for longer than a maximal storage time in order to optimize the secret key rates or almost entirely suppress dephasing errors. In our model, for comparison with the dimensionless "repeaterless" bound (secret key capacity), the finally considered secret key rates per channel use and per mode are also dimensionless and not expressed in Hz. Thus, clock rates given in Hz only have an indirect effect on the QR performance via the accumulated dephasing times and the corresponding variations of the required cutoff. We consider two different protocols, one of which is better adapted to the higher source clock rate and lower memory coherence time of the quantum dot platform. The other protocol, however, circumvents the need of writing the transmitted optical quantum states into the memories in a heralded, nondestructive fashion. It will become apparent that for both protocols, in principle, the elementary building blocks can be connected in a modular fashion to construct a QR system that is potentially scalable to larger distances. Let us now first introduce a minimal set of experimental parameters that can be used to quantitatively assess the performance of a memory-based QR system.

2. Minimal Set of Experimental Parameters Characterizing QR Performance

We assess the performance of a single QR cell (as it will be defined in Section 3) or, similarly, a two-segment QR in a simplified

model applicable to all three physical platforms. For this purpose, we choose three experimental parameters that are primarily related to the sources', the detectors', and the memories' efficiencies: the zero-length channel or link coupling efficiency, P_{link}, the source/memory clock time τ_{clock} (time span between two trigger/excitation events or memory write-in and reset time),[29] and the memory coherence time τ_{coh}. The link coupling efficiency P_{link} incorporates the photon creation efficiency, fiber channel in- and outcoupling efficiencies, and, depending on the protocol, a detector efficiency or a memory write-in efficiency; the fiber channel transmission efficiency η will be treated separately from P_{link}. We consider sources generating true single-photon states as obtainable from initial entangled spin–photon resources. A single photonic qubit that is launched into the fiber channel is encoded into two field modes (typically corresponding to polarization or time-bin encoding). Such single-photon-based two-mode qubits can be easily "rotated" into any qubit state and measured in any qubit basis; for two qubits simple partial Bell-state measurements are available. These single-photon qubit states are also most robust against path length fluctuations along the optical channels and compatible with the stationary matter qubits (as opposed to weak coherent states or other phase-sensitive single-mode states, although also for this case repeater protocols exist[23]). The memory coherence time τ_{coh} is defined via the time-dependent probability for a random phase flip to occur on a memory qubit, $\frac{1}{2}(1-\exp(-\frac{t}{\tau_{\text{coh}}}))$, see Section S2 (Supporting Information). In addition, we include a memory cutoff time, i.e., a maximally allowed storage time until any quantum memory is reset and reinitialized. For a summary of the relevant experimental parameters and our notation used throughout the paper, see Section S1 (Supporting Information).

Let us briefly discuss the influence of the finite link coupling and channel transmission efficiencies in an idealized general QR, without errors and for an arbitrary number of stations/segments, on the QR performance, corresponding to a raw rate in the QKD context. We can then compare this with a quantum PPL, i.e., a scheme without the use of quantum memories solely based on direct transmission of quantum states. A single QR segment can be thought of as a quantum PPL over distance L/n when the total channel of length L is divided into n segments. The raw rate in Hz, i.e., the number of (quantum) bits (secret bits in QKD without errors) per time and per mode, for one segment is then given by

$$\mathcal{R}_{\text{link}}(L/n) = \frac{R_{\text{link}}(L/n)}{NT_0} \tag{1}$$

where R_{link} is the overall (dimensionless) link efficiency,[30] T_0 is the time duration between two channel uses (i.e., time consumed per use), and N is the number of modes in case that several modes are sent in parallel through the optical channel. In general, $R_{\text{link}}(L/n)$ may exceed unity, but it must necessarily remain smaller than one either for not too short segment lengths (i.e., channel segments with more than 3 dB transmission loss for each[12]) in a single-mode link or for an optical encoding based on discrete qubit states, as it applies to our two-mode-qubit-based schemes. This is why we refer to $R_{\text{link}}(L/n)$ as an efficiency and we may decompose it into the two contributions coming from the link coupling and channel transmission efficiencies

$$R_{\text{link}}(L/n) = P_{\text{link}}\eta^{1/n} \tag{2}$$

where, more specifically, the second factor describes the channel transmission in a single repeater segment $\eta^{1/n} = \exp[-(L/n)/L_{\text{att}}]$ (i.e., η is the probability that a single-photon two-mode qubit remains intact after its parallel transmission over two independent amplitude damping channels of length L, while $\sqrt{\eta}$ represents the amplitude damping parameter of a Gaussian single-mode loss channel of length L).

If we connect the segments without the use of quantum memories like in a relay, effectively multiplying the efficiencies of the individual segments, we obtain at best $(R_{\text{link}}(L/n))^n = (P_{\text{link}})^n(\eta^{1/n})^n = (P_{\text{link}})^n\eta$. Since this scales with distance like a PPL over the whole channel, we may just remove the intermediate stations to obtain $R_{\text{link}}(L) = P_{\text{link}}\eta =: R_{\text{PPL}}(L)$. This link efficiency for the total two-mode PPL, up to a factor of 1.44 and for small $P_{\text{link}}\eta$, can also be identified as a "realistic repeaterless" bound for a single-mode channel of length L including a finite link coupling efficiency for the quantum PPL between Alice and Bob with finite source, fiber coupling, and detector efficiencies at Alice's and Bob's stations. For the raw rate in Hz (per mode) obtainable over the whole channel, we can now also write $\mathcal{R}_{\text{PPL}}(L) = R_{\text{PPL}}(L)/NT_0 = (P_{\text{link}}\eta)/NT_0$. In this case, if Alice directly sends a qubit to Bob over the entire distance, she will use $N = 2$ modes for a two-mode-encoded photonic qubit and she may also send many qubits sequentially at a high source clock rate $(\tau_{\text{clock}})^{-1} \sim$ GHz such that the final rate $\mathcal{R}_{\text{PPL}}$ is ultimately limited only by η since $T_0 = \tau_{\text{clock}}$ (also assuming sufficiently fast detectors at Bob's station).

Once quantum memories are employed at the intermediate stations, in principle, a raw rate in Hz (per mode) for the total distance scaling as $\mathcal{R}_{\text{QR}} \sim (P_{\text{link}}\,\eta^{1/n})/NT_0$ can be approached (at fixed n), which corresponds to an expression similar to that for the rate in a single QR segment. The quantity P_{link} is once again the link coupling efficiency related with a single repeater segment and recall that we do not consider additional success probabilities from entanglement purification and swapping in the present discussion on an idealized QR. However, P_{link} should now also contain any inefficiencies related to the light–matter interface or the memory write-in for one segment. Even more important, compared with a memoryless quantum PPL bridging the total distance, the time unit for one channel use T_0 (as only for a PPL uniquely defined and coinciding with the source/detector clock time) will be significantly larger than a source clock time τ_{clock}. For the memory-based QR, depending on the specific protocol, T_0 must include the local memory write-in and reset times ($\sim$ MHz^{-1}) and the necessary waiting times for classical signals announcing successful quantum state transmissions. Thus, although typically one also has $N = 2$ modes for the optical qubits, beating even the realistic "repeaterless" bound expressed in Hz requires a sufficiently long distance such that the superior scaling of $\eta^{1/n}$ dominates over the inferior "clock rate" of the memory-based repeater. So it is important to recognize that even the ideal memory-based QR, compared to a quantum PPL with fast sources and detectors, starts with a "repeater disadvantage," and only for sufficiently large distances can this be converted into a

"repeater advantage." If errors are included, no longer all transmitted (quantum) bits (when employed for QKD) can be turned into secret bits. Related with this, for large distances, the QR rates drop further due to the need of probabilistic quantum error detection (such as entanglement purification) on higher repeater levels (alternatively, as said before, quantum error correction may be employed for all local gate and memory errors).

Note that all-optical quantum repeaters (at least those that work entirely without feedforward operations at the intermediate stations) can, in principle, operate at the same clock rate as a direct-transmission PPL. However, not only do we need rather complicated encoded states for this approach but also typically (though not necessarily) many optical modes $N > 2$ are required to transmit a logical qubit. Therefore, also in this case, sufficiently many segments have to be concatenated to benefit from the better effective transmission per segment, $(R_{\text{link}})'(L/n)$, compared to the long-distance PPL that works with $N = 2$. Such a better effective transmission due to quantum error correction at every station requires sufficiently short segment lengths, as opposed to the schemes we consider here. For short segment lengths, as already mentioned above, non-qubit-based schemes would in principle even allow for a "link efficiency" greater than one corresponding to the transmission of more than a single qubit (secret bit) per channel use.[31] A unique exception is the twin-field QKD concept, for which we also have a high clock rate, only limited by lasers and detectors, and even just a single mode $N = 1$ for the optical transmission. However, this approach is not known to be scalable beyond $\sqrt{\eta}$.[32]

To conclude, beating the (realistic) dimensionless "repeaterless" bound by means of a multimode memory-based quantum repeater with an effective overall transmission efficiency R_{QR}, i.e., effectively exceeding the overall efficiency of a multimode direct-transmission PPL

$$R_{\text{QR}}(L) > 1.44\ N\ P_{\text{link}}\ \eta = 1.44\ N\ R_{\text{PPL}}(L) \gtrsim (N/2)\ \ R_{\text{PPL}}(L) \qquad (3)$$

is the minimal requirement even for a small-scale quantum repeater module to eventually be able to obtain better rates $\mathcal{R}$ in Hz for large-distance quantum communication with many modules than what is obtainable via a long-distance PPL. Here, N is the number of modes and $R_{\text{PPL}}(L) = P_{\text{link}}\ \eta$, as introduced earlier, refers to a two-mode direct-transmission PPL that covers the total channel and employs no quantum memories at all. Thus, here the link coupling efficiency contains only source (with fiber incoupling) and detector (with fiber outcoupling) efficiencies, $P_{\text{link}} = P_{\text{source}}\ \eta_{\text{det}}$. The factor 1/2 in the lowest bound above has been included to stress that $R_{\text{PPL}}(L)$ represents a two-mode link efficiency. The bound in the middle is the (realistic[33]) multimode "repeaterless" bound for large L. In other words, overcoming the dimensionless bounds with a small, elementary repeater is the first necessary condition to be met for an experimental demonstration of in-principle scalable quantum repeater functionality. In our schemes, the QR stations are connected by optical two-mode channels, hence $N = 2$. In this case, overcoming the direct-transmission efficiency bound expressed by a two-mode PPL corresponds to $R_{\text{QR}}(L) > R_{\text{PPL}}(L) = P_{\text{link}}\ \eta$. In our quantitative comparison later (Figures 5 and 7), we will consider as a figure of merit the SKR in a memory-based QR scheme per channel use and per mode. Up to the secret key fraction factor that includes the effect of the dephasing errors for a chosen QKD protocol (see Section S2, Supporting Information), SKR then corresponds to $R_{\text{QR}}(L)/2$. The relevant benchmarks will be the ideal "repeaterless" bound (single-mode secret key capacity), $-\log_2(1-\eta)$, and SKR for a "realistic" but error-free PPL (per channel use and per mode), $R_{\text{PPL}}(L)/2 = P_{\text{link}}\ \eta/2$. Yet ultimately, a comparison must rely on rates in Hz, per time and per mode: $\mathcal{R}_{\text{QR}}$ versus $\mathcal{R}_{\text{PPL}}$.

To sum up, for a given channel transmission efficiency (with $L_{\text{att}} = 22$ km), we consider three fundamental parameters:

1) The link efficiency R_{link}, which is composed of the link coupling efficiency P_{link} (now also including memory efficiencies) and the channel transmission efficiency per segment $\eta^{1/n}$,
2) The memory coherence time τ_{coh}, which can influence both the repeater raw rates and the secret key fraction in the QKD context, and
3) The clock time τ_{clock}, which, depending on the protocol, can have a significant impact even on the dimensionless repeater rates, namely, indirectly in the presence of memory dephasing.

In the following, we will discuss in detail several variants of small-scale proof-of-principle repeater protocols which can be classified into basically two distinct classes: node sends photons ("NSP") and node receives photons ("NRP"). For each protocol we will then specify the particular form of the above three fundamental parameters, especially decomposing the link efficiency into further experimental parameters depending on the protocol. Eventually, we will be able to insert particular values for each of the three hardware platforms in order to compare their possible present and future repeater performances.

3. QR Cell: A Generic Experimental System Showing QR Functionality

Before introducing the basic concept of a QR cell in detail, and applying it to two different protocols and three different physical platforms, let us start by summarizing the overall concept for establishing a QR within our framework:

- A quantum channel is realized by an optical fiber.
- Intermediate stations along the channel include sources of single/entangled photons or spin–photon entanglement, beam splitters, detectors, possibly wavelength converters.
- The "repeaterless" bound limits the (secret key) rates in point-to-point communication (direct transmission without intermediate stations).
- The QR segments create entanglement of two spatially separated quantum memories connected by a direct quantum channel.
- The QR cells consist of two half QR segments with a central QR node containing quantum memories.

As described in the Introduction, the focus here is on fiber channels with a fixed channel attenuation. In our model, the quantitative effect of wavelength converters can be absorbed into P_{link} via a wavelength conversion efficiency (see Section S6, Supporting Information). While Figure 2 shows how entangled QR

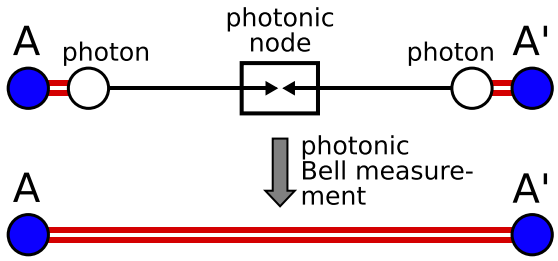

Figure 3. Entanglement creation within a QR segment (with QR nodes sending photons like in the "NSP" protocol below). At the end nodes spin–photon entanglement (full-open pair of circles) is generated. An optical Bell-state measurement on photons arriving at the central photonic node produces entanglement of the end nodes. This configuration does not yet exploit the storage capabilities of the quantum memories, since the photons need to arrive simultaneously at the middle station.

segments, once they are available, can be connected by entanglement swapping to increase the distance of a QR, **Figure 3** illustrates how a single QR segment itself, defined as an entangled pair of quantum memories located at neighboring repeater stations, may be established via an optical BM on two photons (two qubits) emitted by the two quantum memories placed each at the end points.[34]

3.1. Protocol 1: Node Sends Photons

3.1.1. Model, Parameters, Modularity, and Rate Analysis

One of the simplest, most generic protocols promising to show the functionality of a memory-based QR system was put forward by Luong et al.[35] This protocol, which we refer to as NSP protocol, is based on an arrangement that we will call a QR cell. Generally, this is an elementary structure that contains the minimal set of components required to show the functionality of a memory-based QR scheme, thus allowing to analyze schemes that can, in principle, overcome the "repeaterless" bound. An additional important property of a QR cell is that concatenation of QR cells renders the system (if, ideally, only affected by channel loss), in principle, scalable (**Figure 4**). This extra feature is needed, as we know that the "repeaterless" bound can be overcome in a restricted (not fully scalable) sense via a middle station not equipped with quantum memories.[14,15] The NSP protocol relies on only a few generic parameters, whose impact on the QR performance can be clearly identified. It thus allows to compare different hardware platforms, including a qualitative and quantitative assessment of their relative strengths and weaknesses.

For a functioning QR cell (Figure 4b), the central node, equipped with a pair of quantum memories, is crucial. It allows to asynchronously establish effective entanglement in the two half segments, although an entangled state will never be physically shared between the end points of a QR cell. Instead, one would measure the optical signals emitted from the central node at the end points of the cell to establish correlations and obtain a secret key. The specific feature of the NSP protocol for the QR cell is that at the central QR node quantum states with spin–photon entanglement are locally created and then the photons are coupled into the communication channels, i.e., the node sends photons toward the detectors placed on the left and right ends of the cell (Figure 4b). The concatenation of several QR cells then involves two-photon interferences to perform optical two-qubit BMs at the photonic nodes (Figure 4a).

Note that similar elementary QR schemes with a single QR node emitting and sending photons were considered in refs. [36,37] (considering a range of experimental parameters similar to ref. [35], however, including additional memory cutoffs, being adapted to the specific hardware platform of NV centers, and, in ref. [37] incorporating the twin-field QKD concept[15] based on single-photon interference).

Let us discuss the underlying model for a QR cell with the NSP protocol in more detail. A single QR cell (Figure 4b) of total length L is composed of a central memory station placed in the middle between two receiving stations each equipped with photon detectors. The conceptually simplest scenario is when the two quantum memories each emit a single photon in two polarization modes entangled with the memory internal state. One photon is sent to the left receiver and the other photon to the right receiver (Figure 4b). The probability for each photon to arrive at its intended detector after travelling over a channel distance $L/2$ is $\exp[-(L/2)/L_{\text{att}}] \equiv \sqrt{\eta}$. Without the use of quantum memories both detectors must click simultaneously for the transmission to succeed, which happens with a probability $\sqrt{\eta}^2 = \eta = \exp(-L/L_{\text{att}})$ corresponding to the direct-transmission efficiency over a distance L. Thus, a single photon could be equivalently sent directly from left to right without the central station. However, by employing quantum memories, once the middle station is informed about the detection of one photon left or right, the respective memory is kept and for the other light-memory pair further attempts are made to eventually have a second photon arriving at its detector and being detected. A final BM on the two quantum memories, effectively swapping the entanglement of the two spin–photon pairs onto the two successfully distributed photons, establishes correlations between the two detectors such that a secret key can be shared provided that noncommuting observables were measured at the photon detectors (like in a BB84 protocol). Thanks to the memories, in principle, the transmission probability for the total distance L then scales as $\sqrt{\eta}$, corresponding to an effective transmission over only half the distance $L/2$.

The most extreme scenario in a QR cell would be to attempt distributing effective entanglement by sequentially (rather than simultaneously) sending photons entangled with memory qubits to the left and to the right (e.g., first to the left), and start sending those photons entangled with a second spin (e.g., the right one) only when the arrival of a photon belonging to the first spin (e.g., arriving at the left detector) was confirmed and the first spin qubit (e.g., the left quantum memory) was determined to be held for storage. Such an approach can be experimentally useful, because the central node may no longer require two distinct memory systems (with the typical example of a single NV center whose nuclear spin with coherence times of the order of seconds allows for efficient storage and whose electron spin with coherence times of the order of milliseconds can be employed as an interface to the optical communication channel;[36,37] another example would be an ion-based quantum memory composed of two ion species where one is adapted for storage and the other for light–matter interfacing[38]).

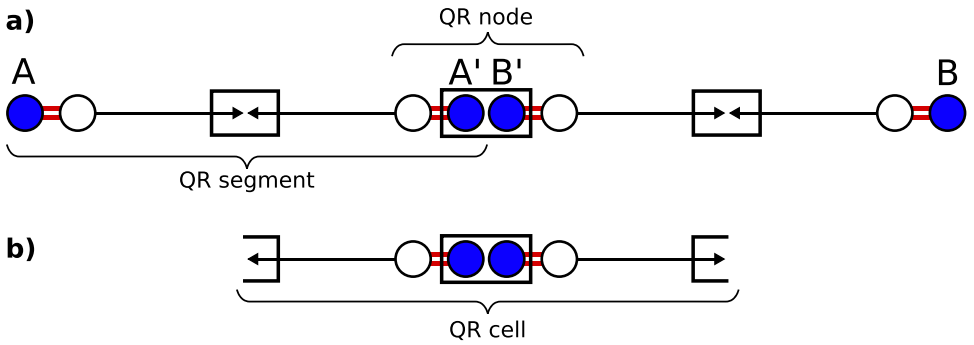

Figure 4. a) Full QR link with two QR segments (NSP) like in Figure 3. b) QR cell (NSP) with two half QR segments and a central node for storage as a minimal element for exploiting memory capability. The pair of quantum memories at the central node enables a valid Bell-state measurement also when the left and right half segments become entangled at different times.

The effective transmission probability R_{QR} is related to the inverse average number of attempts it takes for successfully transmitting the photons to both ends. However, besides this average number, the ultimate secret key (or qubit) rate of a repeater scheme expressed in secret bits (or qubits) per second, $\mathcal{R}_{\mathrm{QR}}$, also depends on the actual duration per attempt (recall the discussion in Section 2). Moreover, the longer a single attempt takes, the smaller the number of attempts becomes that can be executed well within a given quantum memory's coherence time. In the NSP protocol, the duration per attempt is distance-dependent, because any new attempt can only be initiated when the classical signal from the detector has been received. Thus, the total duration of a single attempt is dominated by this waiting time that includes quantum and classical signal transmissions, $T_0 = \frac{L}{c}$ for the QR cell (Figure 4b) and $T_0 = \frac{L}{2c}$ for the two-segment setup in Figure 4a assuming the same total distance L in either case. Hence, the influence of an increased experimental clock rate $(\tau_{\mathrm{clock}})^{-1}$ for preparing spin–photon entanglement and emitting a photon is less significant for the NSP protocol. More precisely, the average dephasing is determined by the factor $\exp(-\frac{T_0}{\tau_{\mathrm{coh}}})$, including the memory- and protocol-dependent quantity τ_{coh}/T_0 that counts how many distribution attempts fit into the given memory coherence time window (see Section S2, Supporting Information). In the NSP protocol, for the QR cell, we have $T_0 = \frac{L}{c} + \tau_{\mathrm{clock}} \approx \frac{L}{c}$ with the relatively large distances that we are interested in.

For the QR cell in the NSP protocol (Figure 4b), we have the link coupling efficiency $P_{\mathrm{link}} = P_{\mathrm{source}}\, \eta_{\mathrm{det}}$ where P_{source} includes all efficiencies related to a source emitting photons entangled with a spin memory and coupling them in (and eventually out of) the fiber channel, i.e., it is the probability to get a photon into and out of a single-mode fiber channel per trigger/excitation event, and η_{det} is the detector efficiency (regarding the effect of wavelength converters, see Section S6, Supporting Information). Constructing two QR segments like in Figure 4a with the NSP protocol corresponds to $P_{\mathrm{link}} = 1/2(P_{\mathrm{source}})^2\ (\eta_{\mathrm{det}})^2$, because one segment is successfully bridged only when both sources at its end points create photons that are both detected at the photonic node in the middle (the factor 1/2 takes into account the efficiency of a standard partial, beam-splitter-based two-photon two-qubit BM). However, the time duration per attempt for one segment of the two-segment scheme (Figure 4a) is half as big as that for the QR cell (Figure 4b) at any given total distance L, as mentioned above.

Table 1. Currently available experimental parameters for the three QR platforms: color centers (NV, SiV), quantum dots, ions (calcium, ytterbium), and atoms (rubidium).

Platform	P_{link} [%]	$(\tau_{\mathrm{clock}})^{-1}$ [MHz]	τ_{coh} [ms]
NV centers[a)]	5	50 (0.5)	10
SiV centers[b)]	5	30 (5)	1
Quantum dots[c)]	10	1000 (32)	0.003
Ions[d)] (Ca/Yb)	25	0.47 (0.007)	20
Atoms[e)] (rubidium)	50	5 (0.005)	100

[a)] Refs. [36,37]; [b)] Refs. [39,40]; [c)] Refs. [41–43]; [d)] Refs. [44–46]; [e)] Refs. [47,48].

Table 2. Potentially available future experimental parameters for the three QR platforms: color centers (NV, SiV), quantum dots, ions (calcium, ytterbium), and atoms (rubidium).

Platform	P_{link} [%]	$(\tau_{\mathrm{clock}})^{-1}$ [MHz]	τ_{coh} [ms]
NV centers[a)]	50	250 (5)	10 000
SiV centers[b)]	50	500 (50)	100
Quantum dots[c)]	60	1000 (323)	0.3
Ions[d)] (Ca/Yb)	50	10 (1)	300
Atoms[e)] (rubidium)	70	10 (1)	1000

[a)] Refs. [36,37]; [b)] Refs. [24,39]; [c)] Refs. [43,49]; [d)] Ref. [50,51]; [e)] Refs. [47,48].

In addition to the three experimentally determined parameters P_{link}, τ_{clock}, and τ_{coh}, we include a memory cutoff parameter imposing the rule that quantum states will never be stored for a longer time than given by the cutoff.[28] In other words, the QR protocol is aborted and started from scratch as soon as a quantum memory's storage time has exceeded the imposed storage limit. The memory cutoff can be freely chosen. Our analysis is based on the experimental parameters for the three platforms as given in the tables next.

Table 1 refers to the state of the art presenting the currently available, realistic values for each platform. **Table 2** shows potential future parameter values, i.e., an idealization compared to the state of the art. Nonetheless, the latter are physically reasonable and not fundamentally unobtainable.

For $(\tau_{\mathrm{clock}})^{-1}$ we list two types of values for all platforms, as will be explained later when we discuss the NRP protocol, because

$(\tau_{\text{clock}})^{-1}$ is not important here for the NSP protocol. Since $(\tau_{\text{clock}})^{-1}$ is of the order of MHz or higher for most platforms, the clock times ∼1 μs or shorter are negligible compared with $\frac{L}{c} \gtrsim 50$ μs for distances $L > 10$ km. The only exceptions are ions and atoms with the longest clock times around 200 μs. For distances $L > 100$ km this also goes below $\frac{L}{c} \gtrsim 500$ μs. Moreover, for smaller distances, the elementary time unit T_0, even including the experimental clock times, is small compared with the values of τ_{coh} assumed for ions and atoms. Overall, $(\tau_{\text{clock}})^{-1}$ plays no significant role in the NSP protocol.

The future parameters of NV centers are obtained by extrapolating the values of refs. [36,37], especially for the link coupling efficiency (and for the clock times as needed later), and assuming a ^{13}C nuclear spin for the memory. Similar assumptions are made for the SiV centers based on refs. [24,39,40]. Compared to NV centers, the SiV platform has the advantage of not only allowing for efficient quantum storage via the nuclear spins but also providing a potentially more efficient photon–spin interface (with higher cooperativities available); though a drawback of SiV is the need for very low temperatures[52] (below 500 mK).[53] Further details regarding the experimentally assumed parameters can be found in Section S6 (Supporting Information).

For the quantum dot platform, based on experimentally achieved quantum dot photon-collection efficiencies of 60%[42] connected with a near Gaussian beam profile which is preferential for large fiber incoupling efficiencies, we estimate the link coupling efficiency P_{link} to 10% (Table 1). Anticipating improvements in photon-collection efficiencies up to 90% together with improved fiber-coupling efficiencies, we assume that a possible future value of P_{link} is 60% (Table 2). Regarding the clock times, we estimate spin-preparation times in a quantum dot to be in the few 100 ps regime, and together with reported radiative recombination times also in the range of a few 100 ps,[43] we expect achievable clock rates of 1000 MHz for a quantum-dot-based nonclassical light source (we refer to Section 3.2 for a further discussion on the impact of experimental clock rates). Additional remarks concerning these experimental parameters can be found in Section S6 (Supporting Information).

We assumed fairly good experimental parameters for the rubidium atom and calcium ion platforms. The presently available values for P_{link} and τ_{coh} refer to current experiments with rubidium atoms in a cavity.[47,48] More specifically, atomic eigenstates can be chosen for the qubit encoding such that the effect of external magnetic fields is significantly reduced. This way coherence times above 100 ms have been measured.[47]

The performance of a QR may be quantified in a meaningful way by the secret key rate that can be obtained for a given length L of the quantum channel connecting the two parties Alice and Bob. The advantage of using the secret key rate as a figure of merit is that it incorporates both the efficiency and the quality (or fidelity) of the quantum state transmission at the same time. A high efficiency, i.e., a high (effective) transmission probability or raw rate leads to an increasing secret key rate, whereas a low fidelity, i.e., a high error rate, results in a decreasing secret key rate (typically incorporated via a secret key fraction). In our rate analysis, we shall consider, on the one hand, secret key rates in an entanglement-based BB84-type scheme, for which optimal memory cutoffs exist, since a cutoff chosen too small will reduce the raw rate and a cutoff chosen too large will lead to a stronger accumulation of dephasing errors reducing the secret key fraction. In other words, the infidelities from the finite coherence times of the memories, eventually becoming manifest as an infidelity of the effective entangled state shared between Alice and Bob after the BM on the memory qubits, are mapped onto a reduced secret key fraction for a BB84 QKD scheme (see Section S2, Supporting Information).

On the other hand, in an alternative picture independent of QKD, we shall only consider the raw rate (without inclusion of dephasing errors) by choosing the cutoff sufficiently small in order to almost entirely suppress dephasing errors and keep the final fidelities of the (effective) entangled state above a certain value such as 0.95. This means the maximally allowed storage time is chosen well below the memory's coherence time for the loaded memory at the central station waiting for the second transmission to succeed. More details can be found in Section S3 (Supporting Information).

It should be stressed that our simplified model does not entirely capture intrinsic effects arising from specific memory errors (beyond pure dephasing) and other error sources for a given hardware platform, such as an imperfect initial spin–photon state prior to its storage-time-dependent dephasing and imperfections of the final two-spin two-qubit BMs, but also detector dark counts. All these additional error sources lead to effective entangled states that are random mixtures of four instead of just two Bell states (see Section S2, Supporting Information) resulting in secret key rates eventually dropping to zero beyond certain distances. An advantage of our simple model, however, is that we are able to use only very few parameters to compare QR schemes employing different hardware realizations with different error mechanisms for the preparation and storage of quantum states. We can then clearly identify which parameter influences the (still to some extent idealized) QR performance in a certain way, mainly manifesting itself in the rate versus distance plot of Figure 1 as a negative offset, i.e., a downshift of the curve due to link coupling inefficiencies, and an increased slope, i.e., an additional distance-dependent rate reduction due to memory inefficiencies.

3.1.2. Results and Comparison for Different Platforms

The resulting raw and secret key rates calculated for our model in the case of the NSP-QR cell (as illustrated by Figure 4b) with the different hardware platforms can be seen in **Figure 5**. The upper part shows the raw rates RR for distributing effective entangled states with a fidelity of at least 0.95 for current (left) and future (right) experimental parameters. The lower part shows the corresponding SKRs. All rates (in dB) are per channel use and per mode (recall the discussion at the end of Section 2).[54]

With current parameters, only the rubidium atom platform enters the repeater regimes. For future values, as calculated, all platforms except for quantum dots enter the repeater regimes. However, the different platforms exhibit a slope increase, i.e., a more rapid decline of the rate with distance, to a different extent in accordance with their ranking in terms of memory coherence time (see Table 2). Apparently, the slope of the rates is clearly connected to the memory efficiencies. The plots cover distances up to 400 km and the curves may be extrapolated to larger distances.

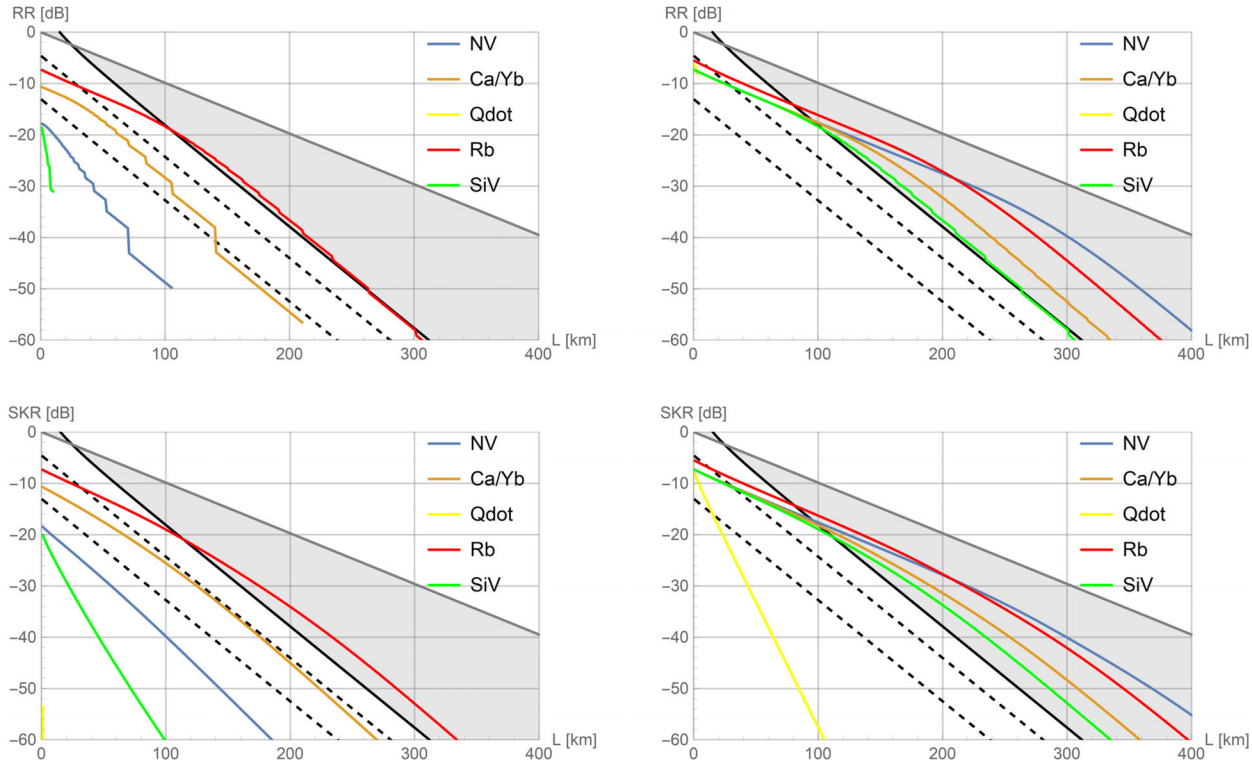

Figure 5. Secret key rates (SKR) and high-fidelity raw rates (RR) for a small NSP-based QR scheme (QR cell). The bottom plots show SKR in dB as a function of the total distance L in km for experimental parameters as currently available (left) and as potentially available in the future (right). The top plots show RR in schemes where the entangled states effectively created over the total distance L have a fidelity of at least 0.95 (left: current parameters, right: future parameters). Curves that are disappearing beyond certain distances (or completely missing for quantum dots) no longer (never) exceed $F = 0.95$. The different platforms correspond to NV (violet) and SiV (green) centers, ions (brown), rubidium atoms (red), and quantum dots (yellow). The light gray area illustrates the (secret key) rate regime between $\sim \eta$ (curve in bold black: "repeaterless" bound) and $\sqrt{\eta}$ (line in dark gray: optimal rate for QR cells or two-segment QR schemes). The bold black dashed lines represent the realistic "repeaterless" bound $P_{\text{link}}\eta/2$ (direct transmission via PPL) with finite link efficiencies $P_{\text{link}} = 0.1, 0.7$.

However, recall that detector dark counts and some other imperfections that could make the rates eventually drop to zero are not included here. The negative offset from the "repeaterless" bounds at zero distance is related to the link coupling efficiency. The quantum dot platform, as calculated here for the NSP protocol, does not enter the repeater regime at all, not even for future parameters (it does though for rather short distances when compared with a "realistic repeaterless" bound as a benchmark that is defined with a smaller link coupling efficiency $P_{\text{link}} = 0.1$). Some curves drop faster than the "repeaterless" bound, which seems contradictory. However, note that even when the very first qubit distribution attempt is successful both memories are already subject to dephasing for one time unit. For platforms with insufficient coherence times, this results in an even steeper decline of the secret key rates compared to the "repeaterless" bound, although the η scaling could be formally attained via the raw rate by not storing the quantum states at all, i.e., setting the cutoff value to zero (see the Supporting Information). All this will become different for another protocol below (NRP) for which, in particular, all platforms are able to access the repeater regimes.

For the NSP protocol, besides a single QR cell (Figure 4b), there is also the variant of a QR with two full segments (Figure 4a). As discussed before, for equal total distance L, the two-segment scheme has a smaller elementary time unit compared to the QR cell ($T_0 = \frac{L}{2c}$ vs $T_0 = \frac{L}{c}$). However, at the same time, the two-segment scheme has a smaller link coupling efficiency ($P_{\text{link}} = 1/2(P_{\text{source}})^2\ (\eta_{\text{det}})^2$ vs $P_{\text{link}} = P_{\text{source}}\ \eta_{\text{det}}$).

For comparison and completeness, we present the rates of the two-segment scheme in Section S4 (Supporting Information).[55] One can see that it performs slightly worse compared to the QR cell. In all plots the secret key rates can sometimes be greater than the raw rates, which again seems contradictory. However, note that for the secret key rates, the optimized memory cutoff (which must neither be too small nor too large to prevent a too small raw rate or a too small secret key fraction, respectively) typically leads to a worst-case fidelity much lower than the minimal fidelity of 0.95 allowed for the calculation of the raw rates alone (requiring a very small memory cutoff to almost entirely suppress dephasing errors).

3.2. Protocol 2: Node Receives Photons

3.2.1. Model, Parameters, Modularity, and Rate Analysis

In order to potentially benefit from a higher source repetition rate as available from the quantum dot platform, we shall consider an alternative NRP protocol (**Figure 6**). In this protocol, photons

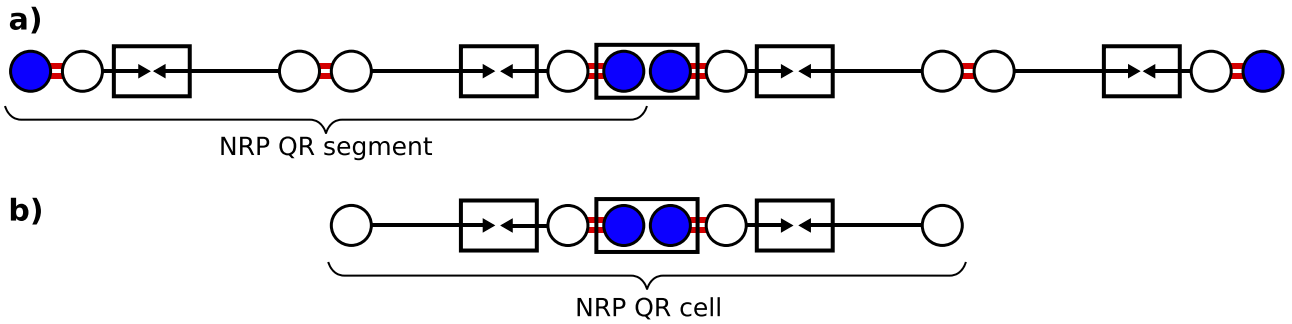

Figure 6. a) Full QR link with two QR segments incorporating the NRP concept. The BMs in Figure 4a are now replaced by Bell-state sources. b) QR cell consisting of two half QR segments and a central node for storage as a minimal element for exploiting memory capability. As opposed to the QR cell in Figure 4b, here the quantum memories "receive" photons from two sending stations; whether a photon has arrived must be confirmed by a nondestructive measurement on the qubit, here realized by a photonic BM on a "local" photon emitted from the memory (open circle) and the photon transmitted through the channel. As before, the final BM on the memories can also be valid when the QR segments become entangled at different times.

are sent from two sending stations to the central memory station where the arrival of a photonic qubit is nondestructively (e.g., by a linear-optics photonic BM teleporting the arriving photonic qubit to the memory qubit) detected before or while it is "written into" the memory. At any failure event, the next photon pulse can be processed with a delay only depending on the repetition rate of the source or depending on the typically longer write-in and reset times of the memory. In this case, the duration per attempt corresponds to the clock time of the source or the write-in time and is independent of the channel distance, $T_0 = \tau_{\text{clock}}$, as opposed to the situation for the NSP protocol where T_0 is mainly determined by the length of the repeater segments.

Thus, the factor that specifies the average memory dephasing (see Section S2, Supporting Information) now becomes $\exp(-\frac{\tau_{\text{clock}}}{\tau_{\text{coh}}})$, while it is now the ratio $\tau_{\text{coh}}/\tau_{\text{clock}}$ that counts the number of distribution attempts fitting into the given memory coherence time. However, note that this feature is specific to a single NRP-QR cell and as soon as several cells are combined into a larger QR system, distance-dependent waiting times for classical signals have to be taken into account again. As a consequence, similar to what holds in general for the case of the NSP protocol, a scalable QR based upon NRP modules (see next) will also be mostly influenced by an experimental improvement of the link coupling efficiency and the memory coherence time, and much less by an enhanced experimental clock time.

A QR cell now still has a central node equipped with quantum memories, but at the end points there are no longer detectors, but sources for optical quantum states such as BB84-encoded single-photon-based qubits (Figure 6b). The memory node now receives the photons. This may be realized by a direct and heralded write-in mechanism (such as those of refs. [56–58]), for which certain write-in inefficiencies and infidelities would apply, or by first preparing spin–photon entangled states at the central node and then coupling the photons near the memories locally with the arriving photons coming from the left and right sources (by an optical BM, see Figure 6b). Similar to the NSP protocol, also QR cells based upon the NRP protocol can be concatenated in order to scale up the QR system to larger distances (Figure 6a). The "photonic nodes" where the half segments meet are now no longer performing BMs like in the NSP case, but are instead equipped with entangled photon pair sources (Figure 6a). Compared to the NRP-based QR cell here, a similar elementary QR scheme with a single QR node receiving photons, for BB84-encoded photonic qubits equivalent to what is referred to as measurement-device-independent QKD[59,60] assisted by a quantum-memory-based middle station, was considered in refs. [61–64] (again mainly adapted to the specific hardware platform of NV centers, but also presenting comparisons with other platforms in ref. [63] and incorporating the idea of a deterministic final BM on the electronic and nuclear spins of a single NV center in ref. [64]).

In order to keep memory dephasing errors small and the fidelity of the effective entanglement shared between Alice and Bob above a certain minimum, in the NSP protocol, for an increasing L a decreasing number of attempts can be executed at a given memory coherence time because of the L-dependence of a single attempt's duration and the growing storage time needed per transmission attempt. In the NRP-protocol-based QR cell (Figure 6b), this L-dependence disappears, since the quantum signals are sent to, and no longer emitted from, the quantum memories. The memory cutoff can be chosen independent of distance and the time duration per transmission attempt can be made arbitrarily small by increasing the repetition rate of the sources up to the local memory write-in and reset times. This means the cutoff (expressed by the number of allowed attempts during one storage cycle) can be chosen much higher resulting in larger raw rates. Moreover, this way the memories have less time to be subject to dephasing during a given number of attempts leading to a larger secret key fraction. Generally, the NSP and NRP protocols have both their benefits and disadvantages. The NSP protocol does not require a nondestructive detection of an arriving photonic qubit or an efficient heralded write-in mechanism, but the memory station has to wait for the classical signals from the receiving detector stations. In contrast, the NRP protocol relies on a nondestructive measurement or any other means to nondestructively write the incoming "flying qubit" into a "stationary qubit" in a heralded fashion; however, there are no extra waiting times for classical signals (as long as we consider the elementary QR cell of Figure 6b). In addition, the NRP scheme inherits all benefits of

measurement-device-independent QKD with an untrusted middle station receiving and measuring the quantum states coming from two outer sending stations.[59–64] For the rate analysis of the NRP-based schemes, the main experimental parameters taken into account in our simple model are the same as for the NSP-based schemes: the link coupling efficiency P_{link}, the memory coherence time τ_{coh}, and the source/memory clock time τ_{clock} which now for the NRP-QR cell may have an actual impact on the repeater performance.

The two types of values given in Tables 1 and 2 for $(\tau_{\text{clock}})^{-1}$ either exclude (numbers without brackets) or include (numbers in brackets) the additional sequences and operations that are typically needed in order to reinitialize a spin every time when an attempted write-in of an arriving photonic qubit failed. Clearly, these numbers differ significantly, and it depends on the particular protocol whether the spin is affected by a failed write-in and has to be reset or not. The specific teleportation-assisted write-in processes as illustrated in Figure 6 would always, in every round, require a newly prepared spin–photon entangled state. However, there are also schemes where the initial spin state is to a great extent only altered at those events when a photonic qubit is actually arriving, ready to be coupled to the spin qubit, and eventually detected (we refer to such schemes as a direct write-in).[24,56–58] Therefore, we will consider both above-mentioned types of values for $(\tau_{\text{clock}})^{-1}$ corresponding to the two extreme scenarios where the experimental clock rate in the NRP protocol is either determined by the repetition rate of a nonclassical source (reaching values as high as 1 GHz for a quantum-dot-based source) or where the necessary spin reset times are fully taken into account.[65] The former scenario is somewhat more general, as it does not rely upon a particular protocol for the spin–photon interface. However, it is idealized assuming an ultrafast write-in mechanism. In our quantitative analysis in Section 3.2.2, we shall combine this idealization with the extra assumption of a deterministic write-in. The complementary scenario of a nondeterministic, slow write-in including memory reset times will be considered in Section S5 (Supporting Information). Further details regarding the experimentally assumed parameters can be found in Section S6 (Supporting Information).

For the QR cell in the NRP protocol (Figure 6b), we now have $P_{\text{link}} = P_{\text{source}}\ P_{\text{write}}$ where P_{source} again includes all efficiencies related to a source emitting photons (this time prepared in BB84 states) and coupling them into (and eventually out of) the fiber channel. The parameter P_{write} represents the probability for successfully writing a photonic qubit arriving at the central node into the respective memory (regarding the effect of wavelength converters, see Section S6, Supporting Information). If a spin–photon entangled state and a linear-optics BM are exploited for this in order to teleport the arriving photonic qubit to the memory spin qubit (see Figure 6b), we have $P_{\text{write}} = 1/2\ P_{\text{source}}(\eta_{\text{det}})^2$ where P_{source} specifically refers to the generation of a spin–photon entangled state. Note that if the BB84-encoded photons were produced in a similar fashion (via initial spin–photon entanglement) with the same source efficiency P_{source}, we would obtain the link coupling efficiency $P_{\text{link}} = P_{\text{source}}\ P_{\text{write}} = 1/2(P_{\text{source}})^2\ (\eta_{\text{det}})^2$, which actually coincides with that of the NSP-based two-segment QR (Figure 4a), because in terms of the link couplings the two schemes become identical when the photonic nodes in the middle of each segment of the NSP scheme both move to the central node right next to the memories (except that the "local" photons may no longer require fiber coupling).[66] For other write-in methods,[56–58] we may just directly insert numbers for P_{write}. Although the two-segment concatenation of NRP-based QR cells and half segments (Figure 6a) demonstrates that the basic modules can be systematically combined to build an in-principle scalable QR system, we shall not consider this scheme in our rate analysis. As opposed to the QR cell in Figure 6b, the combined scheme in Figure 6a does require classical communication to inform the two central memories about the successful loading of their memory counterparts with photons originating from the same entangled photon pair, and thus it will have smaller rates than the QR cell alone (in this context, however, see also the discussion on quantum repeater design presented in ref. [67]). More theoretical details can be found in Sections S2 and S3 (Supporting Information).

3.2.2. Results and Comparison for Different Platforms

The resulting raw and secret key rates calculated for our model in the case of the NRP-QR cell (as illustrated by Figure 6b) with the different hardware platforms can be seen in **Figure 7**. The upper part again shows the raw rates for distributing effective entangled states with a fidelity of at least 0.95 for current (left) and future (right) experimental parameters. The lower part again shows the corresponding secret key rates. All rates (in dB) are again per channel use and per mode (recall the discussion at the end of Section 2). The plots in Figure 7 are for a deterministic memory write-in scheme, $P_{\text{write}} = 1$. Moreover, as for the values given in Tables 1 and 2 for $(\tau_{\text{clock}})^{-1}$, the rates in Figure 7 have been calculated excluding additional spin sequences (numbers without brackets).[68]

This time we observe that already with current parameters all platforms enter the repeater regimes. With future parameters, for the simple model used in the rate calculations (no dark counts and no depolarizing errors), all platforms achieve a rate slope $\sim\sqrt{\eta}$ over the entire distance of 400 km as shown, thus fully exhibiting the repeater advantage. This also holds in particular for the quantum dot platform that, though having the worst memory coherence time, can fully benefit in the NRP protocol from the highest clock rate (see Table 2).

For the NRP-QR cell, we may then also consider an explicit write-in mechanism in the form of a linear optical BM (Figure 6b). In this case, instead of assuming unit write-in efficiency like for the rates calculated in Figure 7, we have $P_{\text{write}} = 1/2\ P_{\text{source}}(\eta_{\text{det}})^2$ as mentioned above. Moreover, the additional sequences for spin reinitialization are included in $(\tau_{\text{clock}})^{-1}$ (numbers in brackets in Tables 1 and 2). We present the corresponding rates calculated for this situation in Section S5 (Supporting Information).

4. Conclusion

As the effective clock rate in a memory-based QKD or QR system is always slower than that of a direct point-to-point quantum connection driven from a laser source at ~GHz rates, the memory-based system will become potentially more efficient only at large

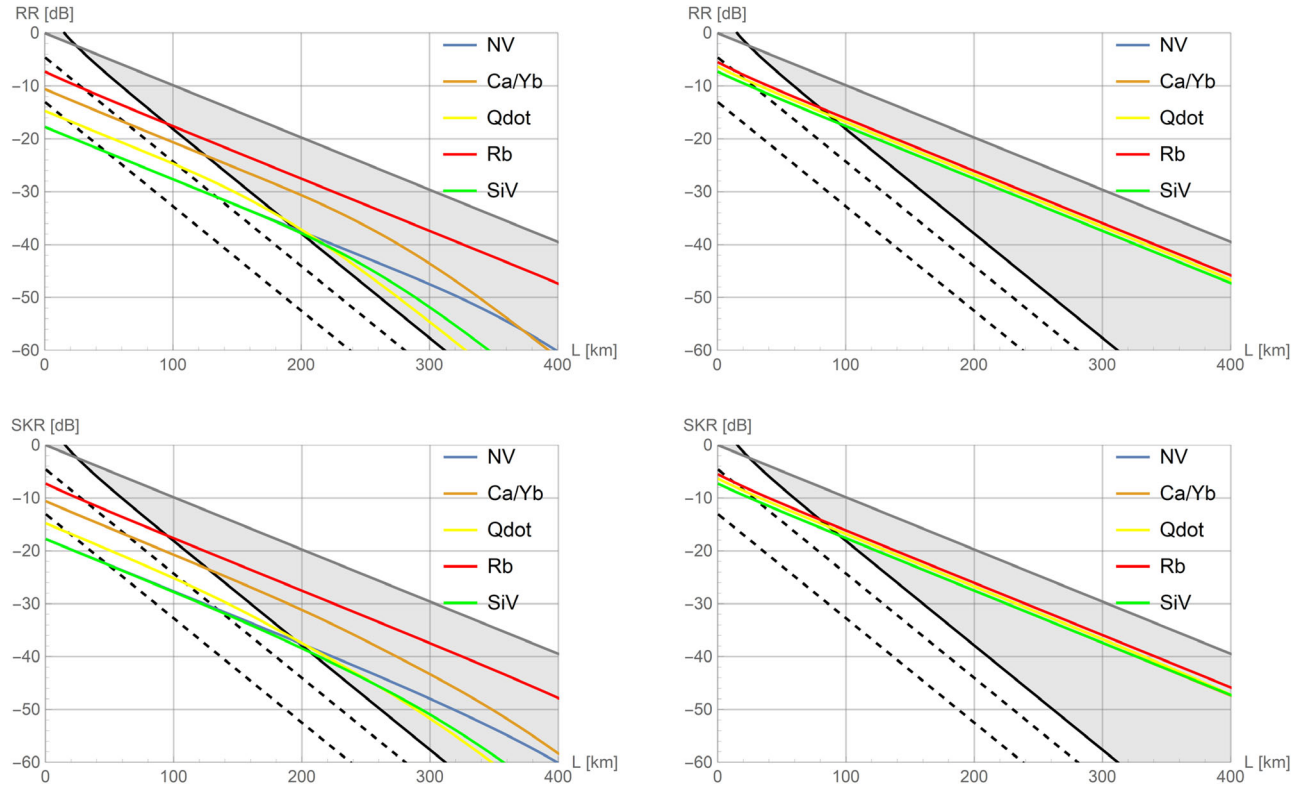

Figure 7. Secret key rates (SKR) and high-fidelity raw rates (RR) for small NRP-based QR schemes (QR cell assuming $P_{\text{write}} = 1$ in $P_{\text{link}} = P_{\text{source}}\, P_{\text{write}}$). The bottom plots show SKR in dB as a function of the total distance L in km for experimental parameters as currently available (left) and as potentially available in the future (right). The top plots show RR in schemes where the entangled states effectively created over the total distance L have a fidelity of at least 0.95 (left: current parameters, right: future parameters). The different platforms correspond to NV (violet) and SiV (green) centers, ions (brown), rubidium atoms (red), and quantum dots (yellow). The NV/ions curves, invisible for future parameters, coincide with those of the other platforms. The light gray area illustrates the (secret key) rate regime between $\sim \eta$ (curve in bold black: "repeaterless" bound) and $\sqrt{\eta}$ (line in dark gray: optimal rate for QR cells or two-segment QR schemes). The bold black dashed lines represent the realistic "repeaterless" bound $P_{\text{link}}\eta/2$ (direct transmission via PPL) with finite link efficiencies $P_{\text{link}} = 0.1, 0.7$.

communication distances requiring sufficiently many elementary QR segments and additional quantum error detection and correction at higher "nesting levels" of the QR. At such large scales, quantum memories must be sufficiently long-lived or fault-tolerant to survive the necessary waiting times especially for the classical signals sent back and forth between the QR stations. However, a necessary requirement for a large-scale QR to show a performance superior to that of direct transmission is that its fundamental elements already exceed the bounds constraining a "repeaterless" system on a smaller scale: employing an elementary QR cell or a two-segment QR should on average lead to a larger secret key or qubit transmission rate than obtainable in a direct transmission. We have investigated such basic elements for a QR system considering two protocol variants for three different hardware platforms.

Combining the basic building blocks in a modular fashion allows to construct a QR system, that is, considering only channel loss, scalable to larger distances. For the realistic situation including general memory and operation errors (such as depolarizing errors with infidelities from the initial states, the light–matter interfaces, and write-in processes, or the spin–spin Bell measurements as well as detector dark counts) eventually additional methods of quantum error correction/detection will be required. Nonetheless, for the small-scale QR elements (cells and two-segment schemes) discussed in this work the impact of both finite link and memory efficiencies (the latter described by a simple dephasing model including a "memory cutoff") on the repeater performance has been analyzed for various hardware platforms. The aim was to keep our model sufficiently simple in order to allow for an analytic treatment and to be able to assess the performances in terms of a small set of experimental parameters. Among the three parameters identified—link coupling efficiency, memory coherence time, and experimental clock rate—most important, especially toward combining the QR modules into a large-scale system, turn out to be the former two parameters. The experimental clock rate specifically influences the performance of our NRP-QR cell.

While, depending on the protocol, some platforms turn out to be superior to others with current and future experimental parameters as assumed in our model, a promising further direction could be a hybridization between the different platforms, for instance, combining the high clock rates of quantum-dot-based sources with the long memory coherence times of rubidium atoms or NV centers. In our NRP protocol, where quantum memories can receive photons at a rate only limited by the source's clock rate and the memory write-in and reset times, but not by the

classical communication times, the "repeaterless" bounds can be exceeded quite comfortably under the assumptions of our simplified model. Even when NRP-based QR cells are connected to reach larger distances, like in our NRP-based two-segment QR scheme using sources of entangled photon pairs, high source clock rates can still be of great benefit.[67] Yet, in general, once QR building blocks are connected to construct a larger system composed of many repeater segments or cells, the classical communication times become a limiting factor in any protocol based on quantum memories.

Ultimately, deciding which quantum communication system performs better for a given range must rely upon rates determined in Hz, i.e., per time in seconds. Nonetheless, for a sufficiently large range, the better effective transmission efficiency of a memory-based QR system that becomes manifest in a scaling-with-distance advantage over any point-to-point link will eventually also lead to higher rates in Hz for the QR. In particular, combining many sufficiently short repeater segments improves the scaling and allows to keep the classical communication times small, provided that errors beyond transmission loss can be dealt with via additional quantum error correction. The resulting rates may still be rather small for a single repeater chain, but they can be increased by operating many chains in parallel or via more advanced multiplexing techniques. Such approaches, besides quantum error correction, can also help to keep memory errors small, thus enhancing the overall secret key rates.

Supporting Information

Supporting Information is available from the Wiley Online Library or from the author.

Acknowledgements

The authors acknowledge support from the BMBF in Germany for the project Q.Link.X.

Open access funding enabled and organized by Projekt DEAL.

Conflict of Interest

The authors declare no conflict of interest.

Keywords

color centers, quantum communication, quantum dots, quantum repeaters, trapped atoms/ions

Received: December 22, 2019
Revised: June 29, 2020
Published online: October 20, 2020

[1] a) V. Scarani, H. Bechmann-Pasquinucci, N. J. Cerf, M. Dušek, N. Lütkenhaus, M. Peev, *Rev. Mod. Phys.* **2009**, *81*, 1301; b) S. Pirandola, U. L. Andersen, L. Banchi, M. Berta, D. Bunandar, R. Colbeck, D. Englund, T. Gehring, C. Lupo, C. Ottaviani, J. Pereira, M. Razavi, J. S. Shaari, M. Tomamichel, V. C. Usenko, G. Vallone, P. Villoresi, P. Wallden, *arXiv:1906.01645*, **2019**.

[2] C. H. Bennett, G. Brassard, in *Proc. IEEE Int. Conf. Computers, Systems and Signal Processing*, Vol. *175*, IEEE, New York **1984**, p. 8.

[3] A. K. Ekert, *Phys. Rev. Lett.* **1991**, *67*, 661.

[4] S. Wehner, D. Elkouss, R. Hanson, *Science* **2018**, *362*, eaam9288.

[5] http://www.chinadaily.com.cn/china/2017-09/30/content_32669593.htm (accessed: October 2017).

[6] a) J. Yin, Y. Cao, Y.-H. Li, S.-K. Liao, L. Zhang, J.-G. Ren, W.-Q. Cai, W.-Y. Liu, B. Li, H. Dai, G.-B. Li, Q.-M. Lu, Y.-H. Gong, Y. Xu, S.-L. Li, F.-Z. Li, Y.-Y. Yin, Z.-Q. Jiang, M. Li, J.-J. Jia, G. Ren, D. He, Y.-L. Zhou, X.-X. Zhang, N. Wang, X. Chang, Z.-C. Zhu, N.-L. Liu, Y.-A. Chen, C.-Y. Lu, R. Shu, C.-Z. Peng, J.-Y. Wang, J.-W. Pan, *Science* **2017**, *356*, 1140; b) G. Vallone, D. Bacco, D. Dequal, S. Gaiarin, V. Luceri, G. Bianco, P. Villoresi, *Phys. Rev. Lett.* **2015**, *115*, 040502.

[7] A. Boaron, G. Boso, D. Rusca, C. Vulliez, C. Autebert, M. Caloz, M. Perrenoud, G. Gras, F. Bussieres, M.-J. Li, D. Nolan, A. Martin, H. Zbinden, *Phys. Rev. Lett.* **2018**, *121*, 190502.

[8] H.-L. Yin, T.-Y. Chen, Z.-W. Yu, H. Liu, L.-X. You, Y.-H. Zhou, S.-J. Chen, Y. Mao, M.-Q. Huang, W.-J. Zhang, H. Chen, M. J. Li, D. Nolan, F. Zhou, X. Jiang, Z. Wang, Q. Zhang, X.-B. Wang, J.-W. Pan, *Phys. Rev. Lett.* **2016**, *117*, 190501.

[9] In combination with transmission losses another limiting factor are dark counts of the detectors. At a distance of 400 km, only ≈ 10 photonic qubits would be transmitted per second when sent at GHz clock rate. Thus, beyond 400 km the optical signals will eventually vanish under dark count noise. In this work, the maximal total distance considered is 400 km, which in the repeater scenario is divided at least into two segments of maximally 200 km length for each.

[10] M. Takeoka, S. Guha, M. M. Wilde, *Nat. Commun.* **2014**, *5*, 5235.

[11] The factor 1.44 stems from the change of base of the logarithm in the Taylor expansion of the secret key capacity, $-\log_2(1-\eta) = -\frac{\ln(1-\eta)}{\ln 2} = \frac{\eta}{\ln 2} + O(\eta^2)$, where $\frac{1}{\ln 2} = 1.442695\ldots$ and $\eta \ll 1$.

[12] S. Pirandola, R. Laurenza, C. Ottaviani, L. Banchi, *Nat. Commun.* **2017**, *8*, 15043.

[13] S. Pirandola, *Commun. Phys.* **2019**, *2*, 51.

[14] K. Azuma, K. Tamaki, W. J. Munro, *Nat. Commun.* **2015**, *6*, 10171.

[15] M. Lucamarini, Z. L. Yuan, J. F. Dynes, A. J. Shields, *Nature* **2018**, *557*, 400.

[16] For a small-scale experiment along the lines of ref. [14], but circumventing such complications, see ref. [69].

[17] Y. Liu, Z.-W. Yu, W. Zhang, J.-Y. Guan, J.-P. Chen, C. Zhang, X.-L. Hu, H. Li, T.-Y. Chen, L. You, Z. Wang, X.-B. Wang, Q. Zhang, J.-W. Pan, *arXiv:1902.06268*, **2019**.

[18] S. Wang, D.-Y. He, Z.-Q. Yin, F.-Y. Lu, C.-H. Cui, W. Chen, Z. Zhou, G.-C. Guo, Z.-F. Han, *arXiv:1902.06884*, **2019**.

[19] X. Zhong, J. Hu, M. Curty, L. Qian, H.-K. Lo, *arXiv:1902.10209*, **2019**.

[20] S. Muralidharan, L. Li, J. Kim, N. Lütkenhaus, M. D. Lukin, L. Jiang, *Sci. Rep.* **2016**, *6*, 20463.

[21] H.-J. Briegel, W. Dür, J. I. Cirac, P. Zoller, *Phys. Rev. Lett.* **1998**, *81*, 5932.

[22] For a summary of our graphical symbols to represent QR elements, see Section S1 (Supporting Information).

[23] N. Sangouard, C. Simon, H. de Riedmatten, N. Gisin, *Rev. Mod. Phys.* **2011**, *83*, 33.

[24] M. K. Bhaskar, R. Riedinger, B. Machielse, D. S. Levonian, C. T. Nguyen, E. N. Knall, H. Park, D. Englund, M. Lončar, D. D. Sukachev, M. D. Lukin, *arXiv:1909.01323*, **2019**.

[25] Therefore, rates expressed in Hz are bounded above by $\frac{c}{L}$ for a total distance L between Alice and Bob if the quality of their finally shared entangled state depends on entanglement purification.[20] For instance, for $L = 1000$ km we obtain a rate clearly below 1 kHz. It is thus useful to first consider small-scale repeaters without purification. For larger scales, one could include purification only at the beginning and otherwise replace it by quantum error correction on the

memories to avoid two-way classical communication over distances beyond one segment length.
[26] Y.-W. Cho, G. T. Campbell, J. L. Everett, J. Bernu, D. B. Higginbottom, M. T. Cao, J. Geng, N. P. Robins, P. K. Lam, B. C. Buchler, *Optica* **2016**, *3*, 100.
[27] However, thanks to recent technological developments typical dark count rates can be reduced dramatically (below 1 dark count s^{-1}).
[28] O. A. Collins, S. D. Jenkins, A. Kuzmich, T. A. B. Kennedy, *Phys. Rev. Lett.* **2007**, *98*, 060502.
[29] Thus, note that τ_{clock} is a parameter that is determined by the experimental hardware. Additional waiting times for classical signals that depend on the type and the arrangement of the repeater protocol will be treated separately.
[30] Generally, R_{link} counts the number of raw (quantum) bits (secret bits) transmitted per channel use in a multimode channel with N modes. It is upper bounded by the multimode secret key capacity $-N\log_2(1-\eta) \approx 1.44\ N\ \eta$.[12]
[31] This is consistent with a general "realistic" quantum PPL-capacity bound[12] in a single-mode QR segment, $-\log_2(1-P_{\text{link}}\ \eta^{1/n})$, that exceeds one for $P_{\text{link}}\ \eta^{1/n} > \frac{1}{2}$ and grows to infinity for $P_{\text{link}}\ \eta^{1/n} \to 1$.
[32] Note that the upper part of Figure 3 below with an appropriate optical encoding, with the memories A and A′ each immediately measured in the BB84 bases, and an optical measurement at the middle station would resemble a twin-field scheme for which a $\sqrt{\eta}$ scaling is ideally attainable.
[33] Note that in our notation for P_{link} we do not make a distinction between links of different mode numbers.
[34] For a summary of our graphical symbols to represent QR elements, see Section S1 (Supporting Information).
[35] D. Luong, L. Jiang, J. Kim, N. Lütkenhaus, *Appl. Phys. B* **2016**, *122*, 96.
[36] F. Rozpędek, K. Goodenough, J. Ribeiro, N. Kalb, V. C. Vivoli, A. Reiserer, R. Hanson, S. Wehner, D. Elkouss, *Quantum Sci. Technol.* **2018**, *3*, 034002.
[37] F. Rozpędek, R. Yehia, K. Goodenough, M. Ruf, P. C. Humphreys, R. Hanson, S. Wehner, D. Elkouss, *Phys. Rev. A* **2019**, *99*, 052330.
[38] S. Santra, S. Muralidharan, M. Lichtman, L. Jiang, C. Monroe, V. S. Malinovsky, *arXiv:1811.10723*, **2018**.
[39] C. T. Nguyen, D. D. Sukachev, M. K. Bhaskar, B. Machielse, D. S. Levonian, E. N. Knall, P. Stroganov, R. Riedinger, H. Park, M. Lončar, M. D. Lukin, *Phys. Rev. Lett.* **2019**, *123*, 183602.
[40] C. T. Nguyen, D. D. Sukachev, M. K. Bhaskar, B. Machielse, D. S. Levonian, E. N. Knall, P. Stroganov, C. Chia, M. J. Burek, R. Riedinger, H. Park, M. Lončar, M. D. Lukin, *Phys. Rev. B* **2019**, *100*, 165428.
[41] D. Press, K. De Greve, P. L. McMahon, T. D. Ladd, B. Friess, C. Schneider, M. Kamp, S. Höfling, A. Forchel, Y. Yamamoto, *Nat. Photonics* **2010**, *4*, 367.
[42] H. Wang, Y.-M. He, T.-H. Chung, H. Hu, Y. Yu, S. Chen, X. Ding, M.-C. Chen, J. Qin, X. Yang, R.-Z. Liu, Z.-C. Duan, J.-P. Li, S. Gerhardt, K. Winkler, J. Jurkat, L.-J. Wang, N. Gregersen, Y.-H. Huo, Q. Dai, S. Yu, S. Höfling, C.-Y. Lu, J.-W. Pan, *Nat. Photonics* **2019**, *13*, 770.
[43] *Quantum Dots for Quantum Information Technologies* (Ed: P. Michler), Springer, New York **2017**.
[44] M. Bock, P. Eich, S. Kucera, M. Kreis, A. Lenhard, C. Becher, J. Eschner, *Nat. Commun.* **2018**, *9*, 1998.
[45] V. Krutyanskiy, M. Meraner, J. Schupp, V. Krcmarsky, H. Hainzer, B. P. Lanyon, *NPJ Quantum Inf.* **2019**, *5*, 72.
[46] D. Hucul, I. V. Inlek, G. Vittorini, C. Cracker, S. Debnath, S. M. Clark, C. Monroe, *Nat. Phys.* **2015**, *11*, 37.
[47] M. Körber, O. Morin, S. Langenfeld, A. Neuzner, S. Ritter, G. Rempe, *Nat. Photonics* **2018**, *12*, 18.
[48] O. Morin, M. Körber, S. Langenfeld, G. Rempe, *Phys. Rev. Lett.* **2019**, *123*, 133602.
[49] H. Bluhm, S. Foletti, I. Neder, M. Rudner, D. Mahalu, V. Umansky, A. Yacoby, *Nat. Phys.* **2011**, *7*, 109.
[50] B. Casabone, K. Friebe, B. Brandstätter, K. Schüppert, R. Blatt, T. E. Northup, *Phys. Rev. Lett.* **2015**, *114*, 023602.
[51] T. G. Ballance, H. M. Meyer, P. Kobel, K. Ott, J. Reichel, M. Köhl, *Phys. Rev. A* **2017**, *95*, 033812.
[52] SiV serves as a representative of a new class of defect centers in solid-state systems (e.g., group IV-vacancy centers in diamond, defects in SiC or hBN and other 2D materials) currently being investigated with the goal of combining long spin coherence times and favorable optical properties. Whether dilution refrigeration systems are a roadblock is a question of the price one is willing to pay to realize a fiber- and memory-based quantum repeater. It will be a general requirement for all solid-state systems to protect them from their surrounding phonon baths.
[53] K.-M. Fu, *Physics* **2019**, *12*, 117.
[54] The apparent discontinuities in the RR curves occur, because the cutoff parameter must always be readjusted depending on distance in order to ensure that a fidelity of at least 0.95 is attained (in particular, the discontinuities are not the result of a numerical simulation; our rate calculations are entirely analytical). For calculating SKR always a fixed cutoff parameter was chosen, although there are actually different optimal cutoffs for different distances. The fixed cutoff was chosen such that over the entire regime of distances, rates cannot be much further improved through cutoff variations.
[55] To be more specific, for obtaining the curves in Figure 5 (QR cell) we directly use the values for P_{link} from Tables 1 and 2. For the curves in Figure S1 (Supporting Information) (two-segment QR), we use the table values for P_{link} squared and multiplied with one half, since $P_{\text{link}} = P_{\text{source}}\ \eta_{\text{det}}$ for the cell and $P_{\text{link}} = 1/2(P_{\text{source}})^2\ (\eta_{\text{det}})^2$ for the two-segment scheme.
[56] N. Kalb, A. Reiserer, S. Ritter, G. Rempe, *Phys. Rev. Lett.* **2015**, *114*, 220501.
[57] C. Kurz, M. Schug, P. Eich, J. Huwer, P. Müller, J. Eschner, *Nat. Commun.* **2014**, *5*, 5527.
[58] C. Kurz, P. Eich, M. Schug, P. Müller, J. Eschner, *Phys. Rev. A* **2016**, *93*, 062348.
[59] H. K. Lo, M. Curty, B. Qi, *Phys. Rev. Lett.* **2012**, *108*, 130503.
[60] S. L. Braunstein, S. Pirandola, *Phys. Rev. Lett.* **2012**, *108*, 130502.
[61] C. Panayi, M. Razavi, X. Ma, N. Lütkenhaus, *New J. Phys.* **2014**, *16*, 043005.
[62] S. Abruzzo, H. Kampermann, D. Bruß, *Phys. Rev. A* **2014**, *89*, 012301.
[63] N. L. Piparo, M. Razavi, W. J. Munro, *Phys. Rev. A* **2017**, *95*, 022338.
[64] N. L. Piparo, M. Razavi, W. J. Munro, *Phys. Rev. A* **2017**, *96*, 052313.
[65] Taking into account the additional spin sequences corresponds to the assumption of τ_{clock} being composed of times for spin initialization (e.g., optical pumping), times for preparing internal degrees of freedom (e.g., generation of a spin superposition state), and the emission times (e.g., on spin-dependent transitions). For further details, see Section S6 (Supporting Information).
[66] From a practical point of view, it appears sensible to assign the same link coupling efficiency to the "local" photons as for those photons that travel through the fiber communication channel, since all sources of loss considered in P_{link} remain present also for the local states in an all-fiber-based setup. Therefore, in our calculations for the NRP-QR cell with teleportation-assisted write-in, we use the same value for P_{link} throughout.
[67] C. Jones, D. Kim, M. T. Rakher, P. G. Kwiat, T. D. Ladd, *New J. Phys.* **2016**, *18*, 083015.
[68] While the assumption of a (near-)deterministic write-in is not so unrealistic, for instance, for the atom platform,[56] another important experimental parameter in this case would be the write-in fidelity, which we do not explicitly include into our simple model here.
[69] Y. Hasegawa, R. Ikuta, N. Matsuda, K. Tamaki, H.-K. Lo, T. Yamamoto, K. Azuma, N. Imoto, *Nat. Commun.* **2019**, *10*, 378.
[70] H.-K. Lo, H. Chau, M. Ardehali, *J. Cryptol.* **2005**, *18*, 133.

[71] L. J. Stephenson, D. P. Nadlinger, B. C. Nichol, S. An, P. Drmota, T. G. Ballance, K. Thirumalai, J. F. Goodwin, D. M. Lucas, C. J. Ballance, *Phys. Rev. Lett.* **2019**, *124*, 110501.
[72] T. Ruster, C. T. Schmiegelow, H. Kaufmann, C. Warschburger, F. S. Kaler, U. G. Poschinger, *Appl. Phys. B* **2016**, *122*, 254.
[73] S. Daiss, S. Welte, B. Hacker, L. Li, G. Rempe, *Phys. Rev. Lett.* **2019**, *122*, 133603.
[74] Gerhard Rempe, private communication.
[75] E. Shchukin, F. Schmidt, P. van Loock, *Phys. Rev. A* **2019**, *100*, 032322.
[76] P. C. Humphreys, N. Kalb, J. P. J. Morits, R. N. Schouten, R. F. L. Vermeulen, D. J. Twitchen, M. Markham, R. Hanson, *Nature* **2018**, *558*, 268.
[77] H. Bluhm, S. Foletti, I. Neder, M. Rudner, D. Mahalu, V. Umansky, A. Yacoby, *Nat. Phys.* **2011**, *7*, 109.
[78] M. Gurioli, Z. Wang, A. Rastelli, T. Kuroda, S. Sanguinetti, *Nat. Mater.* **2019**, *18*, 799.
[79] D. Huber, M. Reindl, Y. Huo, H. Huang, J. S. Wildmann, O. G. Schmidt, A. Rastelli, R. Trotta, *Nat. Commun.* **2017**, *8*, 15506.
[80] Y. Chen, M. Zopf, R. Keil, F. Ding, O. G. Schmidt, *Nat. Commun.* **2018**, *9*, 2994.
[81] F. B. Basset, M. B. Rota, C. Schimpf, D. Tedeschi, K. D. Zeuner, S. F. Covre da Silva, M. Reindl, V. Zwiller, K. D. Jöns, A. Rastelli, R. Trotta, *Phys. Rev. Lett.* **2019**, *123*, 160501.
[82] M. Zopf, R. Keil, Y. Chen, J. Yang, D. Chen, F. Ding, O. G. Schmidt, *Phys. Rev. Lett.* **2019**, *123*, 160502.
[83] J. Zhang, J. S. Wildmann, F. Ding, R. Trotta, Y. Huo, E. Zallo, D. Huber, A. Rastelli, O. G. Schmidt, *Nat. Commun.* **2015**, *6*, 10067.
[84] R. de Sousa, S. D. Sarma, *Phys. Rev. B* **2003**, *68*, 115322.
[85] D. A. Gangloff, G. Éthier-Majcher, C. Lang, E. V. Denning, J. H. Bodey, D. M. Jackson, E. Clarke, M. Hugues, C. L.e Gall, M. Atatüre, *Science* **2019**, *364*, 62.
[86] K. M. Weiss, J. M. Elzerman, Y. L. Delley, J. Miguel-Sanchez, A. Imamoğlu, *Phys. Rev. Lett.* **2012**, *109*, 107401.
[87] H. Wang, Y.-M. He, T.-H. Chung, H. Hu, Y. Yu, S. Chen, X. Ding, M.-C. Chen, J. Qin, X. Yang, R.-Z. Liu, Z.-C. Duan, J.-P. Li, S. Gerhardt, K. Winkler, J. Jurkat, L.-J. Wang, N. Gregersen, Y.-H. Huo, Q. Dai, S. Yu, S. Höfling, C.-Y. Lu, J.-W. Pan, *Nat. Photonics* **2019**, *13*, 770.
[88] J. Liu, R. Su, Y. Wei, B. Yao, S. F. C. D. Silva, Y. Yu, J. Iles-Smith, K. Srinivasan, A. Rastelli, J. Li, X. Wang, *Nat. Nanotechnol.* **2019**, *14*, 586.
[89] H. Wang, H. Hu, T.-H. Chung, J. Qin, X. Yang, J.-P. Li, R.-Z. Liu, H.-S. Zhong, Y.-M. He, X. Ding, Y.-H. Deng, Q. Dai, Y.-H. Huo, S. Höfling, C.-Y. Lu, J.-W. Pan, *Phys. Rev. Lett.* **2019**, *122*, 113602.
[90] S. Unsleber, Y.-M. He, S. Gerhardt, S. Maier, C.-Y. Lu, J.-W. Pan, N. Gregersen, M. Kamp, C. Schneider, S. Höfling, *Opt. Express* **2016**, *24*, 8539.
[91] J. Iles-Smith, D. P. S. McCutcheon, A. Nazir, J. Mørk, *Nat. Photonics* **2017**, *11*, 521.
[92] H. Snijders, J. A. Frey, J. Norman, V. P. Post, A. C. Gossard, J. E. Bowers, M. P. van Exter, W. Löffler, D. Bouwmeester, *Phys. Rev. Appl.* **2018**, *9*, 031002.
[93] T. Gissibl, S. Thiele, A. Herkommer, H. Giessen, *Nat. Photonics* **2016**, *10*, 554.
[94] T. van Leent, M. Bock, R. Garthoff, K. Redeker, W. Zhang, T. Bauer, W. Rosenfeld, C. Becher, H. Weinfurter, *Phys. Rev. Lett.* **2020**, *124*, 010510.
[95] J. H. Weber, B. Kambs, J. Kettler, S. Kern, J. Maisch, H. Vural, M. Jetter, S. L. Portalupi, C. Becher, P. Michler, *Nat. Nanotechnol.* **2019**, *14*, 23.
[96] A. Dréau, A. Tchebotareva, A. El Mahdaoui, C. Bonato, R. Hanson, *Phys. Rev. Appl.* **2018**, *9*, 064031.